Updated version for re-submission femn14.tex

Magnetic order and local spin correlations in $\mathbf{a{-}(Fe_{1-x}Mn_x)_{78}Sn_2Si_6B_{14}}$

A. Kuprin, D. Wiarda*, and D. H. Ryan

Physics Department and Centre for the Physics of Materials, McGill University, 3600 University Street, Montreal, Quebec H3A 2T8, Canada

(December 16, 1999)

Abstract

^{57}Fe and ^{119}Sn Mössbauer spectroscopy has been used to study local spin correlations in site-frustrated $a{-}(Fe_{1-x}Mn_x)_{78}Sn_2Si_6B_{14}$ alloys. Comparison of total magnetisation, hyperfine fields at the magnetic Fe and non-magnetic Sn sites shows that the Mn moments order anti-parallel to the majority Fe moments and that the order established at the transverse spin freezing transition, T_{xy}, exhibits strong antiferromagnetic correlations in the plane perpendicular to the ferromagnetic axis. This result stands in strong contrast with the bond-frustrated case of $a{-}Fe_{100-x}Zr_x$, but is fully consistent with recent numerical simulations of short-ranged models. The clear difference between site- and bond-frustrated systems below T_{xy} demonstrates the importance of short-range interactions in real spin glass systems.

76.80.+y 75.50.Bb 75.50.Lk

INTRODUCTION

The infinite-ranged interactions implicit in mean-field spin glass models [1] make all forms of exchange frustration equivalent. However, real systems are generally dominated by shorter-ranged interactions, and for the case of first-neighbour-only exchange coupling, two distinct situations can be identified: (i) bond frustration and (ii) site frustration.

Bond frustration arises when each exchange bond to a moment's nearest neighbours may be either positive (i.e. ferromagnetic: FM) or negative (i.e. antiferromagnetic: AF). Perhaps the best experimental example of this case is provided by iron-rich a$-$Fe$_{100-\mathrm{x}}$Zr$_\mathrm{x}$ [2,3]. Here the competing exchange interactions arise from the distance dependence of the direct Fe–Fe exchange coupling ($J(r)$) combined with the distribution of nearest-neighbour distances inherent to the glass structure. With no frustration, the material is a ferromagnet, with infinite ranged correlations and collinear order. As frustration is introduced, the order at $T = 0$ becomes increasingly non-collinear and the magnetisation is reduced. The ground state appears to be an xy–spin glass co-existing with perpendicular ferromagnetic order (i.e. along the z–axis). On heating from zero temperature, the xy–spin glass melts at T$_\mathrm{xy}$ to form a collinear ferromagnet with substantial transverse degrees of freedom that fluctuate rapidly and time-average to zero. Further heating takes the system to T$_c$ where the ferromagnet undergoes a conventional 3–D Heisenberg phase transition to a paramagnetic state. As the degree of frustration increases, the features characteristic of ferromagnetic order decline (both T$_c$ and magnetisation fall) while spin-glass character becomes more pronounced (T$_\mathrm{xy}$ rises and irreversibilities at low temperatures become stronger). Eventually, T$_c$ and T$_\mathrm{xy}$ meet, and further increase in frustration lead to a pure 3–D spin-glass (SG) with a transition temperature (T$_\mathrm{sg}$) that is largely independent of the frustration level. The experimental observations [3] are in quantitative agreement with Monte Carlo simulations of a bond-frustrated Heisenberg spin system [4].

Site frustration is achieved by introducing a dopant with AF coupling to all of its nearest neighbours so that the frustration is introduced site-wise rather than bond-wise. While the gross magnetic behavior is essentially the same as the bond frustrated case (the system exhibits non-collinear order at low temperatures, there are two magnetic transitions at intermediate dopings and a spin glass at higher dopings), numerical simulations show that there are two striking differences [5]. Firstly, low levels of doping do not cause frustration. Isolated AF-coupled sites simply order anti-parallel to the majority FM order, reducing the total magnetisation, but not causing any non-collinearity. Frustration only appears when the dopant density is high enough for AF–AF pairs to occur. Secondly, the transverse correlations below T_{xy} exhibit short-range AF character rather than forming the xy–spin glass observed in the bond frustrated case.

Manganese-doped systems provide the most obvious experimental examples of site frustration, and behavior consistent with the numerical simulations is clearly seen. The amorphous (Fe,Mn)–G alloy series represent a highly studied example of site frustration. Typically they contain 75–80 at.% metals with the balance being made up from a mixture of glass-former elements (B, Al, C, Si, Sn and P). Two magnetic transitions are observed beyond the threshold for the appearance of frustration, and these transitions merge at high Mn doping to yield a spin glass. Indeed, the strong similarities in the phase diagrams of a$-(Fe_xMn_{1-x})_{75}P_{16}B_6Al_3$ [6–10], a$-(Fe_xMn_{1-x})_{75}P_{15}C_{10}$ [11], a$-(Fe_xMn_{1-x})_{77}Si_{10}B_{13}$ [12] and a$-(Fe_{1-x}Mn_x)_{78}Sn_2Si_6B_{14}$ [present work] serves to emphasize that it is the frustration introduced by the Mn that dominates the magnetic response and that the properties of the glass-former mix are largely unimportant. Crystalline $Fe_{3-x}Mn_xSi$ yields a very similar phase diagram [13], but also provides a direct confirmation of AF ordering perpendicular to the dominant FM order at T_{xy} [14]. Polarized neutron scattering in an applied field on a single crystal of Fe_2MnSi showed that the transverse spin components that order at T_{xy} are indeed orthogonal to the FM order established at T_c and they exhibit AF correlations, in full agreement with the predictions of the numerical simulations [5].

We present here a study of magnetisation and transferred hyperfine field data for a series of a$-(Fe_{1-x}Mn_x)_{78}Sn_2Si_6B_{14}$ samples doped with ^{119}Sn in order to determine the nature of the local spin correlations that develop at T_{xy}. The results show that the Mn moments order antiparallel to the FM order of the Fe moments, and that in the composition range where two transitions occur, the transverse correlations are indeed AF over the first two neighbouring shells.

EXPERIMENTAL METHODS

The alloys were prepared by arc-melting the appropriate ratio of pure elements (Fe: 99.95%, Mn: 99.9%, B 99.99% and Si 99.999% pure) with isotopically separated ^{119}Sn under Ti-gettered argon to yield $\sim$3 g ingots. Melt-spinning was carried out under a partial pressure of Helium onto a copper wheel at 55 m/s. Absence of crystallinity was confirmed using Cu$-K_\alpha$ powder x-ray diffraction, thermogravimetric analysis (TGA) in a small field gradient, and room temperature Mössbauer spectroscopy.

Magnetisation (shown in Fig. 1) and susceptibility data were obtained on a commercial system in fields of up to 9 Tesla over the temperature range 5 – 300 K. Curie temperatures were obtained from $\chi_{\rm ac}$, bulk magnetisation and Mössbauer spectroscopy for those samples that ordered below 300 K, and by TGA in the cases where T$_c$ was above 300 K.

Mössbauer measurements were made on a constant acceleration spectrometer with a 1GBq ^{57}Co**Rh** source for ^{57}Fe and a 0.1 GBq Ba^{119m}SnO$_3$ source for ^{119}Sn. All spectra were calibrated using an $\alpha-$Fe foil. Samples were mounted in a vibration-isolated closed-cycle fridge for spectra at temperatures down to 12 K. Representative ^{57}Fe and ^{119}Sn Mössbauer spectra for the alloys studied here are shown in Figs. 2 and 3 respectively. The spectra were fitted using an asymmetric Gaussian distribution of hyperfine fields with independent widths above and below the most probable field. This was found to be the simplest, stable, form that would reproduce the observed spectra. A linear correlation between $B_{\rm hf}$ and the isomer shift was included to account for the slight asymmetry in the spectra. A Gaussian distribution of quadrupole splittings was used to fit those spectra obtained above T$_c$. All isomer shifts quoted here are relative to α-Fe at RT.

BASIC CHARACTERISATION

Magnetisation at 5 K (Fig. 1) shows the evolution from square, readily saturated ferromagnetic behavior to highly curved with reduced saturation as the Mn content is increased and the system evolves from ferromagnet to spin glass. Magnetic transition temperatures (derived from both bulk magnetic, ^{57}Fe Mössbauer measurements and TGA, and shown in Fig. 4) show the expected rapid decline in T_c and the appearance of T_{xy}. The results shown in Figs. 1 and 4 are in good agreement with the results of studies on other a–(Fe,Mn)–G systems [6,9,11,12].

The average isomer shift $<\delta>$ reflects the total density of s electrons at the site of a probe nucleus and thus provides information about electronic configuration and chemical bonding. On warming from 12 K to RT $<\delta>_{\rm Fe}$ dropped from 0.24 ± 0.03 mm/s to 0.10 ± 0.04 mm/s (^{57}Fe) and $<\delta>_{\rm Sn}$ dropped from 1.78 ± 0.02 mm/s to 1.70 ± 0.04 mm/s (^{119}Sn).This is consistent with the contribution from the second order Doppler shift and in accordance with data for ^{57}Fe in a$-(\rm Fe_x Mn_{1-x})_{75}P_{15}C_{10}$ [11] and ^{119}Sn in iron [15]. $<\delta>_{\rm Fe}$ also dropped slightly with increasing manganese content x with a fitted slope of $0.0015(2)\ \rm mm\,s^{-1}(at.\%)^{-1}$. This is consistent with a transfer of Fe$-3d$ electrons to the Mn $d-$band [16,17] leading to a reduced shielding of $3s$ and $4s$ electrons [18]. By contrast, $<\delta>_{\rm Sn}$ is essentially constant (data are presented in Table 1), implying that the bonding of the tin atoms is not significantly affected by addition of manganese. The average quadrupole splitting $<\Delta>$, which reflects departures from spherical symmetry in the local chemical environment, is not affected by Mn additions for either ^{57}Fe or ^{119}Sn. This observation, coupled with the weak effects on $<\delta>$ points to the essentially unchanged electronic configuration of both tin and iron atoms with addition of manganese in the range of interest.

The average hyperfine fields ($<B_{\rm hf}>$) at the ^{57}Fe and ^{119}Sn sites provide complementary information on the microscopic ordering of moments in these alloys. For the purpose of the present study it is natural to distinguish (see one of the first reviews on hyperfine interactions in iron based alloys [19]) between the local contribution to the hyperfine field on ^{57}Fe which arises from the total magnetic moment μ_{loc} of the probe iron atom, and non-local contributions, from surrounding magnetic atoms via conduction electron polarization. For ^{119}Sn, which is non-magnetic, the hyperfine field is transferred from moments associated with the magnetic atoms: both nearest neighbour and in more distant coordination spheres [20–23]. Mössbauer probe atoms with zero intrinsic magnetic moment (e.g. ^{197}Au) have been used as an indicator of local correlations in the directions of moments on Fe atoms in **Au**Fe spin glass alloys [24]. The approach was extended to the use of ^{119}Sn for the same system in [25], and applied later to amorphous iron-rich metallic glasses [26–30].

The temperature dependence of $< B_{\mathrm{hf}} >$ for ^{57}Fe and ^{119}Sn shows a clear break in slope for all but the most Mn–rich and Mn–poor alloys. This behaviour is expected, as it is only for intermediate Mn–contents (and hence intermediate frustrations) that two magnetic transitions (T_c and T_{xy}) are predicted [5]. The increase in $< B_{\mathrm{hf}} >$ with no increase in magnetisation on cooling through T_{xy} is characteristic of transverse spin freezing and reflects the ordering of spin components in the xy–plane perpendicular to the FM order established parallel to, and defining, the z–axis at T_c [31]. Starting with the ^{57}Fe data, presented in Fig. 5, those alloys that exhibit no break in slope were fitted using a modified Brillouin function that includes the effects of exchange variations [32]. These fits yield T_c and the average hyperfine field due to the ferromagnetic order along the z–axis extrapolated to T = 0 K: $< B^z_{\mathrm{hf}} >$. The break in slope was modeled by including a second modified Brillouin function to obtain fitted values for $< B^{\mathrm{tot}}_{\mathrm{hf}} >$, the total hyperfine field extrapolated to T = 0 K. However, we found that a linear increase in $< B_{\mathrm{hf}} >$ gave a better fit near T_{xy}, and this form was used to determine T_{xy}. The average transverse field arising from the xy–components of the magnetic moments can be calculated from:

$$(< B^{xy}_{hf} >)^2 \ = \ (< B^{tot}_{hf} >)^2 \ - \ (< B^{z}_{hf} >)^2.$$

The behavior of the field at ^{119}Sn sites shows similar compositional behaviour, with kinks at approximately the same temperature seen for ^{57}Fe. However, there is a strong deviation from a Brillouin-like course in the form of a much steeper decline in comparison with ^{57}Fe

(Fig. 6). This is well known in crystalline magnetic alloys, where the difference between the reduced hyperfine field and the reduced magnetization of the host is called the 'temperature anomaly'. This anomaly introduces an additional uncertainty into the determination of $< B_{\rm hf}^{z} >$ and hence of $< B_{\rm hf}^{\rm xy} >$ for ^{119}Sn in samples that exhibit kinks in $< B_{\rm hf} >$(T). In these cases the value of $< B_{\rm hf}^{z} >$ at T = 0 K was estimated from the value at $\mathrm{T} = 0.5\,\mathrm{T}_c$ where $B_{\rm hf}(T) \sim\ 0.85\, B_{\rm hf}(0)$ according to experimental data on ^{119}Sn in iron ferromagnets [21,22].

The results of fits to both the ^{57}Fe and ^{119}Sn data are given in Table 1. The fitted fields are plotted *vs.* x in Fig. 7. The phase diagram for this system (Fig. 4) is consistent with those of similar amorphous FeMn–G systems (e.g. a$-(\mathrm{Fe_xMn_{1-x}})_{75}\mathrm{P_{16}B_6Al_3}$ [10] and a$-(\mathrm{Fe_xMn_{1-x}})_{77}\mathrm{Si_{10}B_{13}}$ [12]). For $x = 0$ and $x = 0.107$ the samples are ferromagnetic for all temperatures below T_c, while for $x = 0.235$ and $x = 0.320$ two magnetic transitions are evident. Finally, for $x \geq 0.385$, the system is a spin glass.

The primary purpose of the present study is use the temperature and composition dependences of the ^{57}Fe and ^{119}Sn hyperfine fields to determine the nature of the ordering that occurs at $\mathrm{T_{xy}}$. The simplest model involves assuming that both fields are dominated by short-range contributions. In such a model, the ^{57}Fe field is assumed to be proportional to the local iron moment only, while in the case of ^{119}Sn the field is attributed to a vector average over the moments in the first coordination shell (the absence of a local moment on the Sn is explicitly assumed here) [28]. This model has been applied to measurements of magnetic and non-magnetic Mössbauer probes in several bond frustrated systems: ^{119}Sn and ^{197}Au in crystalline $\mathrm{AuFe_{19}Sn_2}$ [24,25] and ^{119}Sn in amorphous $\mathrm{Fe_{92}Zr_7Sn_1}$ [26] and $\mathrm{Fe_{90-x}Ni_xZr_7Sn_1}$ with $x = 1$ and $x = 3$ [30]. In all cases the ratio:

$$\mathcal{R}(T) \ = < B_{hf}^{non-mag} > / < B_{hf}^{Fe} >$$

was found to be constant, or only weakly temperature dependent ($< 10^{-3}\, K^{-1}$). Furthermore, even in the **Au**Fe alloys where a clear break in the temperature dependence of $< B_{\rm hf} >$ was observed for both the magnetic and non-magnetic probes at $\mathrm{T_{xy}}$ [24,25], no break in the slope of $\mathcal{R}(T)$ was present [26]. The observed proportionality between intrinsic field on ^{57}Fe and the transferred field on the non-magnetic probe, leads, within this simple model, to the conclusion that the transverse components are aligned FM over first neighbour distances. A result that is inconsistent with the absence of an increase in magnetisation below T_{xy}, and is in direct conflict with both mean field calculations [1] and numerical simulations [4] which predict SG ordering of transverse components. However, the clearest indication that this simple model is inadequate comes from ^{119}Sn–doped a$-$Fe$_{90}$Sc$_{10}$ [29]. This material is a spin glass with no net magnetisation [27,33], so a zero, or at least very small, transferred field is expected at ^{119}Sn and $\mathcal{R}(T)$ should also be close to zero. However, $\mathcal{R}(T)$ was found to be the same as it is in $\alpha-$Fe and the simple model clearly needs to be improved.

$\mathcal{R}(T)$ for the alloys studied here is shown in Fig. 8. Two features are immediately apparent: (i) there is a systematic increase in the ratio with increasing Mn content, which extends even to the $x = 0.450$ case that is a spin glass. This increase in $\mathcal{R}(T)$ with x both above and below T_{xy} occurs even as the average magnetisation clearly falls (see Fig. 1), and the ^{57}Fe field drops by a factor of 4.5 (see Fig. 5). These results serve to underline the inadequacy of the simple model outlined above. (ii) There is a clear break in the slope of $\mathcal{R}(T)$ for $x = 0.235$ and $x = 0.320$, the two alloys which exhibit transverse spin freezing. No such break has been observed in previous studies of bond frustrated alloys and this is strong evidence that the detailed nature of the ordering at T_{xy} in these site frustrated materials differs from the bond frustrated case.

ANALYSIS OF TRANSFERRED HYPERFINE FIELDS

For the purpose of the present study of the hyperfine fields at the Mössbauer probe sites we will use the approach of a magnetic polarization model (see detailed analysis in [34]) which distinguishes between contributions local to the magnetic moment of Mössbauer probe atom and those transferred from magnetic moments on neighboring atoms. Both types of contribution act through the polarization of s–like electrons via exchange interactions with unpaired $3d$ electrons. The net polarization at the probe nucleus then induces a hyperfine field through the Fermi contact interaction.

Within this model, the average field at the nucleus of a magnetic probe atom (^{57}Fe) in an amorphous magnetic alloy in which different magnetic species are uniformly distributed over coordination spheres, may be written as a sum of two components. The first is associated with the local magnetic moment of the probe, while the second reflects the contribution from surrounding magnetic atoms:

$$< B_{hf}(Fe) > = \ A < \mu_{loc} > \ + B < \mu_1 >, \qquad (1)$$

where A and B are constants, $< \mu_{\rm loc} >$ is the magnetic moment of the probe atom (which may be affected by the species present on neighboring sites [34]) and $< \mu_1 >$ is the average moment of surrounding atoms, with the main contribution to it coming from the first nearest neighbours (1$^{\rm st}$ NN) [34]. Unfortunately, consistent values for A and B are not directly available from the literature. The theoretical problem is challenging, and as yet unsolved. Comparisons are further complicated because the decomposition terms used (core, valence, conduction electron polarisation etc.) do not map uniquely onto Eqn. 1. Also most work is on collinear magnetic systems, where the only real constraint is provided by the sum $A+B$, and separating the two contributions is complex. Theoretical estimates for A range from 10 T/μ_B for Fe–V sandwiches [35], 7–10 T/μ_B for FeCr and FeCo alloys [36] to 3.7 T/μ_B for impurities in nickel [37]. Experimental values include the widely-used 15 T/μ_B (all local, no transferred field), 7.5 T/μ_B in (Fe,Mn)$_3$Al [38], 4 T/μ_B at ^{55}Mn in the same alloy [39], to zero, due to a cancellation of two local terms, derived for Fe-Al alloys [40].

Since there is no consunsus, we adopt the following procedure to determine A and B. The first term is entirely local and the prefactor A should not be affected by chemical or magnetic environments. Its value can be estimated from experimental data on the hyperfine field at the Cu nucleus in dilute **Fe**Cu alloys. Since there is no local moment on the Cu, the observed hyperfine field of -21.3 to -21.8 T [41–43] represents the effects of non-local transferred hyperfine fields. Dividing by the Fe moment of $2.2\,\mu_B$ gives $B = \ -9.9$ T/μ_B.

Substituting this value for B and the the -34.0 T hyperfine field observed for Fe in bulk iron at 4.2 K into Eqn. 1 yields $A = 5.5$ T$/\mu_B$. It is important to note that the model used here differs significantly from that used previously [26,28], as over 60% of the observed ^{57}Fe field now derives from the influence of the first neighbours. The second term in Eqn. 1 involves transferred fields and is in principle affected by the density of conduction electrons, and hence, the value of $B = -9.9\,\mathrm{T}/\mu_B$ derived from bulk Fe may not always apply. Indeed, when this two-component model was applied to a variety of ferromagnetic iron based alloys a value of $B = -8.0\,\mathrm{T}/\mu_B$ [44] was reported. Using the fact that in the $x = 0$ alloy, the iron moment is equal to the value of bulk magnetisation per magnetic atom (data on measured and calculated moments are summarized in Table II) and that for this case $\mu_1 = \mu_{\mathrm{Fe}}$ we obtain $B = -7.22 \pm 0.18\,\mathrm{T}/\mu_B$ which is slightly smaller than reported in other alloys [44].

Since the ^{119}Sn probe has no local moment, the $< \mu_{\mathrm{loc}} >$ term for ^{119}Sn must be zero, and any observed hyperfine field must be due entirely to the influence of neighbouring moments. Any hyperfine field must arise from a polarisation of occupied inner electron shells, and it has been shown experimentally that the hyperfine field on ^{119}Sn can be represented as a sum of two contributions of opposite sign [20–23]. The positive term originates from a direct interaction between polarized conduction band electrons and electrons of the filled Sn shells, while the negative term comes from an indirect polarization of the internal shells by polarized outer shell electrons [20]. The two terms are large and close in absolute magnitude and are in turn made up of sums of partial contributions from different coordination spheres. The negative, indirect term, is much more local in nature and the positive, direct term, prevails by the second sphere [21–23]. This combination leads to oscillations in the radial dependence of the partial contribution to the total hyperfine field and makes the net field very sensitive to the distribution of magnetic moments over the coordination spheres. It is this sensitivity that we exploit here to determine the nature of the order below $\mathrm{T_{xy}}$. The radial dependence of the partial contributions to the total hyperfine field at ^{119}Sn has been determined experimentally [45, and references therein] by analyzing data from *bcc*, *fcc* and *hcp* metallic ferromagnets with different distributions of magnetic moments over the coordination spheres. Analysis of such data with the explicit assumption that the net contribution to the field from moments in spheres with radius larger than 4 Å can be represented by a single term proportional to the average magnetisation of the alloy (σ) shows that the resultant transferred hyperfine field is negative for $r < 2.8$ Å, has a sign reversal at $r \sim 2.9 - 3.2$ Å, reaches a positive maximum for $r \sim 3.5$ Å, and crosses the axis again around 3.8 Å. The corresponding dependence for ^{57}Fe atoms in *bcc* alloys is quite similar, except that the negative contribution from nearest neighbours always dominates.

If we approximate the rather complex form described above by using two terms, the first (negative) term being due to moments in the first coordination shell, and the second (positive) term coming from all moments in more distant coordination shells, then we obtain a two-component model similar to that used for ^{57}Fe above, except that the first term of Eqn. 1 is explicitly zero (no ^{119}Sn moment) and the second term is now broken up into the first coordination sphere and beyond. This two component model has previously been used to explain the large temperature anomalies in the hyperfine field (due to a strong radial dependence of the negative contribution to the field), the correlation between temperature anomalies and thermal expansion of the lattice, and the strong pressure dependence of the field in metallic ferromagnets [46, and references therein]. Self-consistent calculations of the electronic structure of *sp* impurity atoms in ferromagnetic iron show a similar separation between the negative contribution to the field arising from bonding states and the positive one due to anti-bonding states, and also that the contribution from core polarization is small [47].

This two-component model leads to the following expression for the average field at the ^{119}Sn nucleus in our amorphous alloys:

$$< B_{\mathrm{hf}}(Sn) > = \ -C < \mu_1 > \ + D\sigma, \tag{2}$$

where C and D are constants [48]. In order to proceed, we need the sign of the hyperfine field at the ^{119}Sn sites, a parameter that cannot be determined uniquely without applying an external field. However, it is reasonable to assume that for $x = 0$ it is negative as it is in

$\alpha-$Fe where $B_{\rm hf}(Sn) = -8.3$ T [21,15]. Furthermore, an inspection of Figs. 1, 7a, and 7b shows that the ^{119}Sn field grows as the average alloy magnetisation falls, suggesting that the negative term ($C < \mu_1 >$) always dominates. Finally, the negative sign of the temperature anomaly apparent in Fig. 6 for $x = 0.235$ requires that the field also be negative for this alloy [46]. Assuming therefore that the ^{119}Sn field is negative, and taking $D = 20\,{\rm T}/\mu_B$ from [45], we derive $C = 22.6 \pm 0.2\,{\rm T}/\mu_B$ for the $x = 0$ alloy. Taking the number of nearest metal neighbours in our alloy to be close to 10 with separation $r \sim 2.57\,$Å (estimated from experimental data on a$-$Fe$_{1-x}$B$_x$ system [49]), we obtain value of partial contribution equal to $2.3 \pm 0.2\,{\rm T}/\mu_B$/neighbour, which is in rather good agreement with the value of $2.1 \pm 0.1\,{\rm T}/\mu_B$/neighbour for $r = 2.59\,$Å derived from data on Sn-doped FeRh and Fe$_3$Ge [45].

The volume expansion caused by introducing Mn [52], coupled with the significant radial dependence of the contribution from the first neighbour shell (about $14\,{\rm T}\,{\mu_B}^{-1}\,$Å^{-1}) [46]) means that B and C, in Eqns. 1 and 2 respectively, must be composition dependent. A further correction should be introduced to account for a linear decrease in the total moment on Fe in accordance with the change of measured and calculated $< \delta >$ [50] (upper estimate of which is ∼10% when half of Fe atoms are replaced by Mn [11]). This decrease in $< \mu_{\rm Fe} >$ also diminishes the contribution to A from $s - d$ mixing, but the change is expected to be much less than 10% and will not be considered here. We emphasise that while these corrections are expected from the origins of the various components and serve to improve the overall consistency of the fits, they do not in any way affect the final conclusions.

DEDUCED MAGNETIC STRUCTURES

Fig. 1 shows that there is a very large reduction in the magnetisation on going from $x = 0$ to $x = 0.107$. If we assume that the magnetic structure remains collinear, then we deduce an average Mn moment $< \mu^z_{\rm Mn} > = -2.89(10)\,\mu_B$ indicating an anti-parallel ordering of the Fe and Mn moments. This is fully consistent with the absence of a second magnetic transition and with model calculations for this composition [5], where the Mn atoms are expected to be surrounded by Fe atoms and Mn–Mn contacts will be absent. We can also estimate the Mn moment from the ^{57}Fe hyperfine field. Eqn. 1 (written now for z–components) gives $< \mu_1^z > = 1.56(5)\,\mu_B$ and assuming additivity in the polarization of conduction electrons by Fe and Mn moments, the longitudinal component of Mn moment can be calculated from the following equation:

$$< \mu_{\rm Mn}^z > = ((1-x) < \mu_{\rm Fe}^z > - < \mu_1^z >)/x, \tag{3}$$

where a positive value for $< \mu_{\rm Mn}^z >$ corresponds to AF Fe–Mn alignment. The deduced value of $< \mu_{\rm Mn}^z > = 3.47 \pm 0.50\,\mu_B$ is somewhat larger than, but consistent with the magnetisation result. This consistency provides an additional check on our selection of values for A and B in Eqn. 1.

Using $< \mu_1^z > = 1.56(5)\,\mu_B$ in Eqn. 2 (also written for z–components) and assuming collinear order, gives $D = 16.7 \pm 0.9\,\mathrm{T}/\mu_B$, which is about 16% smaller than the value for the alloy without Mn. This decrease reflects the assumption that the net contribution to the field from magnetic moments located at distances larger than 4 Å (i.e. from all shells following the 1$^{\rm st}$ NN shell) can be written as a single term proportional to σ. However, the majority of this term comes from the 2$^{\rm nd}$ NN shell, and the z–component of its average moment will be closer to $< \mu_1^z >$ than to σ, the former being about 8% smaller (data are summarised in Table II). Thus the apparent drop in D stems from a limitation of the model, however, a complete accounting for further shells would introduce unwarranted complications.

The alloys with higher Mn contents are expected to have non-collinear magnetic structures [5] and both the $x = 0.235$ and $x = 0.320$ samples exhibit the two magnetic transitions characteristic of partially frustrated systems (see Figs. 4 and 5). Equations 1 and 2 will be true for the z– components of the fields and moments, but when applied to $< B_{\rm hf}^{\rm tot}(Fe) >$ and $< B_{\rm hf}^{\rm tot}(Sn) >$ respectively they should be regarded as a vector equations i.e. they should involve a dependence on the angle (α) between vectors $< \mu_{\rm Fe}^{\rm tot} >$ and $< \mu_1^{\rm tot} >$, and the angle (θ) between vector $< \mu_1^{\rm tot} >$ and the z–direction defined by the domain magnetization.

Thus:

$$(< B_{hf}^{tot}(Fe) >)^2 \ = \ (A < \mu_{Fe}^{tot} >)^2 \ + \ (B < \mu_1^{tot} >)^2 \ + \ 2AB < \mu_{Fe}^{tot} >< \mu_1^{tot} > \cos\alpha \quad (4)$$

and

$$(< B_{hf}^{tot}(Sn) >)^2 \ = \ (C < \mu_1^{tot} >)^2 \ + \ (D\sigma)^2 \ - \ 2CD < \mu_1^{tot} > \sigma\cos\theta \quad (5)$$

To proceed further, we need to assume a form for the correlations between the transverse spin components. Two simple possibilities exist: collinear and random. The former can be further broken down into ferromagnetic and antiferromagnetic. FM alignment of transverse components would lead to a net increase in magnetisation and can, in principle, be eliminated from consideration immediately. However in what follows, we will retain this case in the interests of completeness. We deal first with the case of collinear ordering of the transverse components and then the random, or spin-glass case.

If we assume collinear alignment of the transverse components of the Fe and Mn moments, then the angles α and θ in Eqns. (4) and (5) are linked via ($\varphi_{\rm Fe}$) the angle between the average Fe moment $< \mu_{\rm Fe}^{\rm tot} >$ and the z–direction:

$$\alpha \ = \ |\theta \ \pm \ \varphi_{Fe}| \, . \quad (6)$$

In the present model, the transverse field on ^{119}Sn arises only from the transverse component of the moments in the 1$^{\rm st}$ NN shell, and the net transverse component of the 2$^{\rm nd}$ and following NN shells as well as that of bulk magnetization is assumed to average to zero. In this case, Eqn. 2 reduces to:

$$< B_{hf}^{xy}(Sn) > = \ C < \mu_1^{xy} >, \quad (7)$$

and $< \mu_1^{\rm xy} >$ can be determined directly from the data. The transverse field on ^{57}Fe will depend on the transverse components of both the local Fe moment and that of the 1$^{\rm st}$ NN shell. Allowing for either FM or AF alignment through the $\pm$ sign in Eqn. 6, Eqn. 2 becomes:

$$< B_{hf}^{xy}(Fe) > = \ A < \mu_{Fe}^{xy} > \ \mp B < \mu_1^{xy} > \quad (8)$$

and allows us to find $<\mu_{\rm Fe}^{\rm xy}>$ using $<\mu_1^{\rm xy}>$ obtained from Eqn. 7. We note that there is no defined direction within the xy–plane and we need only to know the respective orientation of transverse components of the moments on Fe and Mn, and hence their absolute values, which, in the approximation of the present model, are connected by an equation analogous to Eqn. 3:

$$<\mu_{Mn}^{xy}> = \ ((1-x)|<\mu_{Fe}^{xy}>| \ \pm \ |<\mu_1^{xy}>|)/x, \tag{9}$$

where again a positive value for $<\mu_{\rm Mn}^{\rm xy}>$ corresponds to AF alignment with respect to $<\mu_{\rm Fe}^{\rm xy}>$.

The two roots of Eqn. 8 mean that two possible configurations of the moments on Fe and Mn can exist with the same values of $<\mu_1^{\rm xy}>$, and $<\mu_{\rm Fe}^{\rm tot}>$. Configurations with AF alignment of $<\mu_{\rm Fe}^{\rm xy}>$ and $<\mu_1^{\rm xy}>$ result in unrealistically large average total moments on Mn of about $6.3 \pm 0.4\,\mu_B$ and thus will not be considered in the following discussion.

Knowing the values of $<\mu_{\rm Fe}^{\rm xy}>$ and $<\mu_{\rm Fe}^{\rm tot}>$ we can determine $<\mu_{\rm Fe}^{z}>$. Then, using Eqn. 1 written for z–components (we assume that $<\mu_{\rm Fe}^{z}>$ points in the positive z–direction) one can find the value and orientation of the longitudinal component of the 1st NN shell moment:

$$<\mu_1^z> = \ (<B_{hf}^z(Fe)> \ - A <\mu_{Fe}^z>)/B, \tag{10}$$

where a negative value for $<\mu_1^z>$ corresponds to AF alignment with respect to $<\mu_{\rm Fe}^{z}>$. Finally, knowing $<\mu_1^z>$, we can calculate the average value of the total moment of the first near-neighbours shell $<\mu_1^{\rm tot}>$.

For the alloy with $x = 0.450$ it is impossible to separate the longitudinal and transverse components of the moments, but the fact that the spontaneous bulk magnetization σ is zero (see Fig. 1 and [11,53]) allows us to derive $<\mu_1^{\rm tot}>$ directly from Eqn. 5. Its use in Eqn. 4 then gives the value of $\cos\alpha$ which can then be used to calculate the average moment on the Mn atoms using an equation analogous to Eqns. 3 and 9 which links average moments $<\mu_{\rm Fe}^{\rm tot}>$, $<\mu_{\rm Mn}^{\rm tot}>$, and $<\mu_1^{\rm tot}>$ and which now becomes a vector equation. We note that direct determination of the proportionality factor D is not possible for the complete spin-glass state, however, apart form this, we are able to determine all of parameters for the present model. The results of this analysis are summarised in Table II.

If we repeat the analysis while assuming a random orientation of $< \mu_{\rm Mn}^{\rm xy} >$ and $< \mu_{\rm Fe}^{\rm xy} >$ for the alloys with $x = 0.235$ and $x = 0.320$, and random orientation of $< \mu_{\rm Fe}^{\rm tot} >$ and $< \mu_{\rm Mn}^{\rm tot} >$ for the complete spin-glass with $x = 0.450$ we obtain values of $< \mu_1^{\rm xy} >$ and $< \mu_1^{\rm tot} >$ that are approximately twice as large as those obtained under the assumption of AF alignment. Furthermore, the assumption of random orientation of $< \mu_{\rm Fe}^{\rm xy} >$ and $< \mu_1^{\rm xy} >$ in Eqn. 8 yields very large values for $< \mu_{\rm Fe}^{\rm xy} >$($1.31 \pm 0.04\, \mu_B$ and $1.81 \pm 0.04\, \mu_B$ for $x = 0.235$ and $x = 0.320$ respectively). The latter value is almost the same as $< \mu_{\rm Fe}^{\rm tot} >= 2.09 \pm 0.01\, \mu_B$. Statistical averaging of $< \mu_{\rm Fe}^{\rm xy} >$ and $< \mu_1^{\rm xy} >$ with weights from Eqn. 9 then leads to very large values for $< \mu_{\rm Mn}^{\rm xy} >$ of $4.35 \pm 0.05\, \mu_B$ and $3.92 \pm 0.05\, \mu_B$ for $x = 0.235$ and $x = 0.320$ respectively. These in turn result in unrealistically large values for $< \mu_{\rm Mn}^{\rm tot} >$ of $5.63 \pm 0.35\, \mu_B$ and $5.20 \pm 0.25\, \mu_B$. Thus we can immediately rule out the possibility of random orientations of either the transverse components or the total moments on Fe and Mn.

Introducing $\varphi_{\rm Mn}$ the angle between the average Mn moment and the $-z$–direction (c.f. $\varphi_{\rm Fe}$ defined above), we find that average total Fe and Mn moments deflect respectively from the $+z$– and $-z$–directions in the opposite half-planes. At $x = 0.235$ their canting angles are close: $\varphi_{\rm Fe} = 29 \pm 4\,^\circ$ and $\varphi_{\rm Mn} = 34 \pm 5\,^\circ$ and weak frustration causes a rather small net canting of $< \mu_1^{\rm tot} >$ ($\theta = 22 \pm 3\,^\circ$). At higher frustration ($x = 0.320$) the canting of the Fe moment increases ($\varphi_{\rm Fe} = 45 \pm 5\,^\circ$), but remains the same for Mn ($\varphi_{\rm Mn} = 33 \pm 3\,^\circ$). Nevertheless the frustration is now strong enough to cause $< \mu_1^z >$ to point in the $-z$–direction, $\theta = 109 \pm 12\,^\circ$.

For the complete spin-glass at $x = 0.450$, Eqn. 4 gives cosα less than -1, due mostly to uncertainties in the determination of $< B_{\rm hf}^{\rm tot}(Sn) >$ and $< \mu_1^{\rm tot} >$ discussed previously. However, we know from the two cases of moderate frustration discussed above, that the Fe and Mn moments are aligned almost completely AF, therefore it seems reasonable to expect this behaviour to continue into the spin-glass regime, so that $< \mu_1^{\rm tot} >$ is oriented completely

AF with respect to $< \mu_{\rm Fe}^{\rm tot} >$. We will take cos$\alpha$ to be -1 in calculations of the total Mn moment at $x = 0.450$.

The most important conclusion of the present analysis is that in partially frustrated alloys the transverse components of the Mn moments $< \mu_{\rm Mn}^{\rm xy} >$ order AF with respect to the transverse components of the Fe moments $< \mu_{\rm Fe}^{\rm xy} >$. This same result was obtained in recent Monte Carlo simulations on a 3-D Heisenberg model with nearest-neighbor interactions on a simple cubic lattice [5], in which site disorder was introduced by randomly replacing a fraction f of FM sites by AF sites. It was shown that in this case frustration can occur only when f is high enough to produce AF–AF nearest pairs which on average start to appear when $f = 1/{\rm NN}$. Increased frustration led to an increases in both the non-collinearity, and $\rm T_{xy}$, and a decrease in $\rm T_{\it c}$. While the longitudinal components of the spins within each sub-lattice were ordered FM on average, the frozen transverse components exhibited short range AF correlations. Comparison of the normalized transverse spin freezing temperatures ($\rm T_{xy}/T_{\it c}$) in Fig. 9 shows that our experimental data are in good agreement with the magnetic phase diagram of the site-disordered model [5]. The exception is the point at $x = 0.385$ which suggests that the system reaches the spin-glass regime earlier than the numerical model. In view of the excellent agreement over the rest of the phase diagram, the most likely explanation for the discrepancy lies with the details of the exchange distribution.

The numerical model assumed a simple $\pm J$ exchange distribution, however this is unlikely to be the case in a real system. Indeed, the steep decline of $\rm T_{\it c}$ with x apparent in Fig. 4 suggests that the AF Mn-Mn interactions are significantly stronger than the FM Fe-Fe interactions. Fitting the concentration dependence of $\rm T_{\it c}$ assuming a simple mixing model [11,56] and temperature independent exchange constants, gives the following values: $J_{\rm FeFe} = 679 \pm 9$ K, $J_{\rm MnFe} = 227 \pm 51$ K, and $J_{\rm MnMn} = -1175 \pm 84$ K, or approximately: $|J_{\rm MnMn}| = 5.2|J_{\rm MnFe}| = 1.7|J_{\rm FeFe}|$ which is in agreement with the ratio obtained for crystalline $\gamma - FeMn$: $|J_{\rm MnMn}| = 6|J_{\rm MnFe}| = 2|J_{\rm FeFe}|$ from measurements of magnetic specific heat [51]. This large variation in exchange strengths has a number of consequences. The existence of distinct Mn and Fe sub-lattices assumed in our analysis and the overall AF

Fe–Mn orientations derived from our analysis both require $|J_{\rm MnMn}|$ and $|J_{\rm FeFe}|$ to be larger than $|J_{\rm MnFe}|$. The greater size of $J_{\rm MnMn}$ also leads to the frustration independent canting angle of the average Mn moment ($\varphi_{\rm Mn}$ remains at $\sim 33\,^\circ$ with x rising from 0.235 to 0.320), while the weaker $J_{\rm FeFe}$ leads to a rapid increase in the canting angle of the Fe moments ($\varphi_{\rm Fe}$ increases from $29\,^\circ$ to $45\,^\circ$). Finally, the greater magnitude of $J_{\rm MnMn}$ means that misaligned Mn moments will have a greater effect on the surrounding moments and so explains why long-ranged order is lost at lower doping levels in the experimental system than in the numerical model where $\pm J$ was used (see Fig. 9). [57]

APPLICATION OF THE MODEL TO OTHER AMORPHOUS ALLOYS

It is interesting to apply the two component model for hyperfine fields on ^{57}Fe and ^{119}Sn used in the present work to other iron-rich Fe glasses. The simplest will be to use it for alloys containing only one magnetic species, (e.g. Fe) where data on both $< B_{\rm hf}(Fe) >$ and $< B_{\rm hf}(Sn) >$ have been obtained on several partially and fully frustrated alloys. Estimates of the ratio $\mathcal{R}(T)$ for the cases of collinear alignment of transverse components can be made from formulae obtained after trivial mathematical transformations of the equations for $< B^{\rm tot}_{\rm hf}(Fe) >$ and $< B^{\rm tot}_{\rm hf}(Sn) >$ (Eqns. 4 and 5 respectively) and by introducing the xy–component of the Fe moment as a fraction q of the total moment assuming that $< \mu^{\rm tot}_{\rm Fe} >$ $= < \mu^{\rm tot}_1 > = \sigma$ in the case of FM alignment:

$$\mathcal{R}_{\rm FM}(T) \;=\; (D \;-\; C)/(A \;+\; B), \tag{11}$$

and $< \mu^z_{\rm Fe} > = < \mu^{\rm tot}_1 > = \sigma$ in the case of AF alignment:

$$\mathcal{R}_{\rm AF}(T) \;=\; \left((D \;-\; C)\sqrt{1 \;-\; q^2}\right)/\sqrt{A^2 \;+\; (B^2 \;+\; 2AB)(1 \;-\; q^2)}. \tag{12}$$

We note that $\mathcal{R}_{\rm FM}(T)$ depends only on the field transfer coefficients, and not on any alloy parameters, while $\mathcal{R}_{\rm AF}(T)$ also depends on q, i.e. larger tilting reduces the influence of the surrounding moments due to cancellation among the transverse components and $\mathcal{R}_{\rm AF}$ falls.

For the case of spin glass alignment of transverse components, we assume that $< \mu_{\rm Fe}^z > = < \mu_1^z > = \sigma$. $< B_{\rm hf}^{\rm tot}(Fe) >$ and $< B_{\rm hf}^{\rm tot}(Sn) >$ can be obtained by statistical averaging of the $xy-$components of the corresponding moments. We find that $\mathcal{R}_{\rm SG}(T)$ also includes a dependence on $< \mu_{\rm Fe}^{\rm tot} >$.

A study of a$-$Fe$_{92}$Zr$_7$Sn showed a temperature independent $\mathcal{R}$, with no apparent anomaly at T$_{xy}$. [26] This was interpreted as indicating locally FM alignment of the transverse spin components. In order to apply our model to this data, we need values for the field transfer coefficients A — D. A sets the local contribution to $< B_{\rm hf}(Fe) >$ from the Fe atom itself, and D gives the contribution to $< B_{\rm hf}(Sn) >$ from domain magnetisation. Both have been found to be independent of the alloy system used, so we have taken the values from the a$-$FeMn alloys studied here, i.e. $A = -5.5\,{\rm T}/\mu_B$, $D = 20\,{\rm T}/\mu_B$. B was then estimated as $-9.5\,{\rm T}/\mu_B$ by applying Egn. 1 to the collinear a$-$Fe$_{89}$Zr$_{11}$ at 5 K where $< B_{\rm hf}(Fe) >= 23.4 \pm 0.2\,T$ and $\mu_{\rm Fe} =< \mu_1 >= 1.56 \pm 0.04\ \mu_B$ [3]. Local AF or SG alignment of xy–components with $q = 0.40$ (found for a$-$Fe$_{92}$Zr$_7$Sn at 5 K [26]) would result in $< B_{\rm hf}^{\rm tot}(Fe) >= 22.0 \pm 0.5\,{\rm T}$ which is somewhat less than the experimental value of $23.7 \pm 0.2\,{\rm T}$ [3], and hence both correlation forms would appear to be unlikely. Assuming local FM alignment of the xy–components and taking $\mathcal{R}_{\mathcal{FM}} = 0.227$ (the average of experimental data obtained for a$-$Fe$_{92}$Zr$_7$Sn in the temperature range from 5 K to 90 K [26]), yields $C = 23.4\,{\rm T}/\mu_B$(from Eqn. 11). The two component model combined with the assumption of local FM alignment of xy–components then predicts the experimentally observed [26] temperature independent $\mathcal{R}$. By contrast, local AF alignment of $xy-$components leads to a ∼2% drop of $\mathcal{R}_{\mathcal{AF}}(T)$ below T$_{xy}$, while local SG alignment leads to a ∼24% increase in $\mathcal{R}_{\mathcal{SG}}(T)$. Thus, combining the measured fields with the observed dependence of $\mathcal{R}_{\mathcal{SG}}(T)$ we find that the experimental data on the bond-frustrated a$-$Fe$_{100-{\rm x}}$Zr$_{\rm x}$ alloys are consistent only with local FM alignment of the transverse spin components.

Substitution of Fe by Ni in a$-$Fe$_{90-{\rm x}}$Ni$_{\rm x}$Zr$_9$Sn leads to a 10% increase in $< B_{\rm hf}^{\rm tot}(Fe) >$ measured at 12 K on going from $x = 0$ to $x = 3$. This change is due to increased collinearity (reflected by a narrowing of the hyperfine field distribution and increased T$_c$) and an increase in the Fe moment (reflected by increased magnetisation) [30]. On going from $x = 1$ to $x = 3$, $\mathcal{R}(T)$ decreases from ~ 0.235 to ~ 0.223 while $< B_{\rm hf}^{\rm tot}(Sn) >$ does not change. This behavior cannot be appropriately accounted for in the one component model which would predict an increase in $< B_{\rm hf}^{\rm tot}(Sn) >$ caused by increases in collinearity and Fe moment. The two component model however, predicts a greatly reduced effect. For locally FM correlations, $< \mu_1 >$ and σ will scale together as the Fe moment increases, and Eqn. 2 shows that $< B_{\rm hf}(Sn) >$ is then to $(D - C)\sigma$. The coefficients are close in size, greatly reducing the effects of an Fe moment increase. Eqn. 11 further shows that changes in collinearity do not affect $\mathcal{R}$. The net effect of the Fe moment increase on adding Ni is therefore a larger $< B_{\rm hf}(Fe) >$ at constant $< B_{\rm hf}(Sn) >$ and so $\mathcal{R}$ decreases.

Finally, we consider the case of fully frustrated a$-$Fe$_{90}$Sc$_9$Sn$_1$ which exhibits a single transition to an isotropic spin-glass state [27]. a$-$FeSc and a$-$FeZr have many similarities including comparable compositions, and atomic radii (1.60 Å for Zr and 1.62 Å for Sc and Sn). The low temperature value of $< B_{\rm hf}^{\rm tot}(Fe) >$ for a$-$Fe$_{90}$Sc$_{10}$ (and a$-$Fe$_{90}$Sc$_9$Sn$_1$) is 22.9 T [54,29], very close to the essentially composition-, and hence frustration-, independent 23.4 T found in a$-$Fe$_{100-\rm x}$Zr$_{\rm x}$ [3,54]. The observation that $< B_{\rm hf}^{\rm tot}(Fe) >$ remains constant in a$-$Fe$_{100-\rm x}$Zr$_{\rm x}$ despite a 30% reduction in σ [3] is only consistent with locally FM correlated transverse components. Any other form would lead to some cencellation and a drop in $< B_{\rm hf}^{\rm tot}(Fe) >$. In view of the many similarities between the a$-$FeSc and a$-$FeZr systems, it seems reasonable to expect that the correlations will continue to be FM as we cross into the spin glass. These expectations can be examined in more detail using the two component hyperfine field model for a$-$Fe$_{90}$Sc$_9$Sn$_1$. $< \mu_1^{\rm tot} >= 0.22 \pm 0.02\,\mu_B$ may be directly obtained from Eqn. 5 (the second term is zero, as the average magnetisation, σ, is zero, and $< B_{\rm hf}^{\rm tot}(Sn) >= 5.1 \pm 0.2\,\rm T$ was measured for a$-$Fe$_{90}$Sc$_9$Sn$_1$ at 12 K). This result is about half the value of $< \mu_1^{\rm tot} >= 0.41 \pm 0.05\,\mu_B$ obtained by isotropic statistical averaging of 12 vectors $< \mu_{\rm Fe}^{\rm tot} >= 1.55 \pm 0.05\,\mu_B$ (using the moment obtained for the collinear a$-$Fe$_{89}$Zr$_{11}$ [3]). This assumption of random orientation also leads to a simulated value for $< B_{\rm hf}^{\rm tot}(Fe) >= 9.1 \pm 0.5\,\rm T$ (isotropic statistical average of the vector A$< \mu_{\rm Fe}^{\rm tot} >$

and resulting isotropic statistical average of 12 vectors B$<\mu_{\mathrm{Fe}}^{\mathrm{tot}}>$) which is again less than half of the value measured experimentally. Therefore, we can conclude that the absence of a bulk magnetisation, σ, does not translate into a fully random orientation of the moment vectors over the 1^{st} NN shell.

CONCLUSIONS

The magnetic properties of site-frustrated a$-(\mathrm{Fe}_{1-\mathrm{x}}\mathrm{Mn}_{\mathrm{x}})_{78}\mathrm{Sn}_2\mathrm{Si}_6\mathrm{B}_{14}$ have been studied as functions of temperature and Mn concentration, x. Specifically, the detailed nature of the short-range correlations that develop below T_{xy} have been investigated using magnetic and non-magnetic Mössbauer probes. At low x, the Mn moments couple AF with respect to the majority Fe moments and the alloy retains its collinear structure. Once x is large enough for Mn–Mn pairs to occur, exchange frustration develops and the magnetic order at T$=0$ becomes non-collinear. On warming, the transverse components that lead to the non-collinearity melt at a well defined temperature T_{xy} and the order is then collinear until it is lost on reaching T_c. The transverse components in this site-frustrated system were shown to exhibit AF correlations below T_{xy}, in strong contrast to the xy–spin-glass order predicted for bond frustrated materials. Furthermore, both the longitudinal '$z-$', and transverse '$xy-$' components of the Fe moments are oriented anti-parallel to their Mn counterparts. Indeed, this anti-parallel tendency is so strong that it persists even in the fully frustrated $x = 0.450$ alloy. The general magnetic behaviour as well as the AF character of the short-range correlations in the $xy-$components are fully consistent with the results of Monte Carlo simulations on a three-dimensional site-disordered Heisenberg model with nearest-neighbor interactions.

We have shown that it is essential to use a two-component model in order to obtain a consistent description of the hyperfine fields at both magnetic and non-magnetic Mössbauer probes. Such a model considers the effects of both the local Fe moment and the average moment on the 1^{st} NN shell on the hyperfine field at magnetic ^{57}Fe sites, and the effects of both 1st NN and more distant shells on the hyperfine field at non-magnetic ^{119}Sn sites. The coefficients A, B, C and D used here, were derived from a variety of experimental syatems as consistent theoretical values are not available. Development of this model has allowed us to complete a rigorous analysis of the transferred hyperfine fields in a$-(Fe_{1-x}Mn_x)_{78}Sn_2Si_6B_{14}$ and so determine the nature of the local correlations among transverse components below T_{xy}. The conclusions of this analysis are robust, and while substantial changes in the field-transfer coefficients in Eqns. 1 and 2 degrade the fit quality and lead to variation in the Fe and Mn moments, they do not change the final result – anti-parallel orientation of the Fe and Mn moments.

We have also applied the two component model to a range of bond-frustrated alloys, and shown that in this case, the transverse correlations below T_{xy} are strongly ferromagnetic in nature, at least on a first-neighbour length scale. In combination with bulk magnetisation data, we can easily distinguish between FM, AF, or SG short-range transverse correlations on a local scale.

ACKNOWLEDGMENTS

This work was supported by grants from: the Natural Sciences and Engineering Research Council of Canada and Fonds pour la formation de chercheurs et l'aide à la recherche, Québec.

REFERENCES

* Present Address: WIARDA, 7520 Wickam Rd., Knoxville, TN 37931

[1] M. Gabay and G. Toulouse, Phys. Rev. Lett. **47** 201 (1981).

[2] D.H. Ryan, Zin Tun, and J.M. Cadogan, J. Magn. Magn. Mater. **177-181** 57 (1998).

[3] H. Ren and D.H. Ryan, Phys. Rev. B **51** 15885 (1995).

[4] J.R. Thomson, Hong Guo, D.H. Ryan, M.J. Zuckermann, and M. Grant, Phys. Rev. B **47** 3129 (1992).

[5] M. Nielsen, D.H. Ryan, Hong Guo, and M. Zuckermann, Phys. Rev. B **53** 343 (1996).

[6] C.L. Chien, J.H. Hsu, P.J. Viccaro, B.D. Dunlap, G.K. Shenoy, and H.S. Chen, J. Appl. Phys. **52** 1750 (1981).

[7] H. Keller, K.V. Rao, P.G. Debrunner, and H.S. Chen, J. Appl. Phys. **52** 1753 (1981).

[8] I. Merebeau, G. Jehanno, I.A. Campbell, F. Hippert, B. Hennion, and M. Hennion, J. Magn. Magn. Mater. **54-57** 99 (1986).

[9] J.A. Geohegan and S.M. Bhagat, J. Magn. Magn. Mater. **25** 17 (1981).

[10] G. Aeppli, S.M. Shapiro, H. Maletta, R.J. Birgeneau, and H.S. Chen, J. Appl. Phys. **55** 1628 (1984).

[11] K. Heinemann, C. Michaelsen, M. Fieber, and K. Bärner, J. Magn. Magn. Mater. **82** 204 (1989).

[12] T. Miyazaki, I. Okamoto, Y. Ando, and M. Takahashi, J. Phys. F **18** 1601 (1988).

[13] S. Yoon and J.G. Booth, J. Phys. F **7** 1079 (1977).

[14] T. Ersez, S.J. Kennedy, and T.J. Hicks, J. Phys.:CM **7** 8423 (1995).

[15] D.C. Price, J. Phys. F **4** 639 (1974).

[16] S.G. Kang, H. Onodera, H. Yamamoto, and H. Watanabe, J. Phys. Soc. Japan **36** 975 (1974).

[17] Y. Nishihara, S. Ogawa, and S. Waki, J. Phys. Soc. Japan **42** 845 (1977).

[18] L.R. Walker, G.K. Wertheim, and V. Jaccarino, Phys. Rev. Lett. **6** 98 (1961).

[19] F. van der Woude, and G.A. Sawatzky, Physics Reports C **12** 335 (1974).

[20] A.E. Balabanov and N.N.Delyagin, Sov. Phys. JETP **27** 752 (1968).

[21] A.E. Balabanov and N.N.Delyagin, Sov. Phys. JETP **30** 1054 (1970).

[22] N.N.Delyagin and E.N. Kornienko, Sov. Phys. JETP **32** 832 (1971).

[23] N.N.Delyagin and E.N. Kornienko, Sov. Phys. JETP **34** 1036 (1972).

[24] M.M. Abd-Elmeguid, H. Micklitz, R.A. Brand, and W. Keune, Phys. Rev. B **33** 7833 (1986).

[25] A. Ait-Bahammou, C. Meyer, F. Hartmann-Boutron, Y. Gros, and I.A. Campbell, J. Phys. (Paris) Colloq. **49** C8-1157 (1988).

[26] H. Ren and D.H. Ryan, Phys. Rev. B **47** 7919 (1993).

[27] H. Ren and D.H. Ryan, J. Appl. Phys. **73**, 5494 (1993).

[28] D. Wiarda, H. Ren, and D.H. Ryan, Hyperfine Interact. **94** 2303 (1994).

[29] D. Wiarda and D.H. Ryan, J. Appl. Phys. **76** 6189 (1994).

[30] D. Wiarda and D.H. Ryan, J. Appl. Phys. **76** 6377 (1994).

[31] D.H. Ryan, in *Recent Progress Progress in Random Magnets*, edited by D.H. Ryan (World Scientific, Singapore, 1992).

[32] K. Handrich, Phys. Stat. Sol. **32**, K55 (1969).

[33] D.H. Ryan, J.M. Cadogan, and S.J. Kennedy, J. Magn. Magn. Mater. **162** 55 (1996).

[34] Brent Fultz, in *Mössbauer spectroscopy Applied to Magnetism and Materials Science*, edited by Gary J. Long and Fernande Grandjean, vol.1 (Plenum Press, New York, 1993).

[35] M.E. Elzain, D.E. Ellis and D. Guenzburger, Phys. Rev. B **34** 1430 (1986).

[36] H. Ebert, H. Winter, D.D. Johnson and F.J. Pinski, J. Phys. CM **2** 443 (1990).

[37] S. Blügel, H. Akai, R. Zeller and P.H. Dederichs, Phys. Rev. B **35** 3271 (1987).

[38] S. Mager, E. Weiser, T. Zemcik, O. Schneeweiss, P.N. Stetsenko and V.V. Surikov, Phys. Stat. Sol. (a) **52** 249 (1979).

[39] M. Wolf, S. Mager, P.N. Stetsenko, V.V. Surikof and S.I. Kasatkin, Sov. Phys. JETP **44** 800 (1976).

[40] S.M. Dubiel and W. Zinn, Phys. Rev. B **26** 1574 (1982).

[41] D.A. Shirley and G.A. Westenbarger, Phys. Rev. **138** A170 (1965).

[42] Y. Koi, A. Tsujimura, T. Hihara and T. Kushida, *Proc. Int. Conf. Magnetism and Crystallography*, (Kyoto, 1961), J. Phys. Soc. Japan **17** Suppl. BI, 96 (1962).

[43] Le Dang Khoi, P. Veillet and I.A. Campbell, J. Phys. F **5** 2184 (1975).

[44] C.C.M. Campbell, T. Birchall, and J.C. Suits, J. Phys. F **7** 727 (1977).

[45] N.N.Delyagin, V.I. Krylov, and V.I. Nesterov, Sov. Phys. JETP **52** 532 (1980).

[46] N.N.Delyagin, Yu.D. Zonnenberg, V.I. Krylov, and V.I. Nesterov, Hyperfine Interact. **11** 65 (1981).

[47] M. Akai, H. Akai, and J. Kanamori, J. Phys. Soc. Japan **54** 4246 (1985).

[48] We explicitly include the '$-$sign' in this equation to emphasise the opposite signs of the two contributions to the ^{119}Sn hyperfine field. This choice makes both C and D in Eqn. 2 positive. We recognise that the hyperfine field at both the ^{57}Fe and ^{119}Sn sites is in fact negative, but omit the many $-$ signs for clarity.

[49] Y. Waseda and H.S. Chen, Phys. Stat. Sol. (a) **49** 387 (1978).

[50] P.H. Dederichs, R. Zeller, H. Akai, and H. Ebert, J. Magn. Magn. Mater. **100** 241 (1991).

[51] T. Hashimoto and Y. Ishikawa, J. Phys. Soc. Japan **23** 213 (1967).

[52] Y. Endoh and Y. Ishikawa, J. Phys. Soc. Japan **30** 1614 (1971).

[53] A.K. Sinha, J. Appl. Phys. **42** 338 (1971).

[54] D.H. Ryan, J.O. Strom-Olsen, W.B. Muir, J.M. Cadogan, and J.M.D. Coey, Phys. Rev. B **40** 11208 (1989).

[55] S. Asano, J. Yamashita, J. Phys. Soc. Japan **31** 1000 (1971).

[56] I.V. Medvedeva, Yu.S. Bersenev, A.A. Ganin, K. Baerner, J.-W. Schuenemann, and K. Heinemann, J. Magn. Magn. Mater. **124** 293 (1993).

[57] The onset of T_{xy} depends only on the presence of Mn–Mn pairs and so is unaffected by relative exchange strengths.

TABLES

TABLE I. Basic characteristics derived from temperature dependencies of the average hyperfine fields on ^{57}Fe and ^{119}Sn in a$-(\mathrm{Fe}_{1-\mathrm{x}}\mathrm{Mn}_{\mathrm{x}})_{78}\mathrm{Sn}_{2}\mathrm{Si}_{6}\mathrm{B}_{14}$ with different compositions: Curie temperature - T_c, the temperature of transverse spin freezing - T_{xy}, the average field in the direction of bulk magnetization $< B_{\mathrm{hf}}^{z} >$ at 12 K, the total average field $< B_{\mathrm{hf}}^{\mathrm{tot}} >$ at 12 K, together with the average isomer shift $< \delta >$ at 12 K, and the average quadrupole splitting Δ at RT.

	x		0.000	0.107	0.235	0.320	0.450	$\pm$
	T_c	(K)	677	509	284	136	31	2
	T_{xy}	(K)	–	–	49	52	31	2
	$< B_{\mathrm{hf}}^{z} >$	(T)	27.9	22.8	14.0	7.4	–	0.2
^{57}Fe	$< B_{\mathrm{hf}}^{\mathrm{tot}} >$	(T)	27.9	22.8	15.8	12.5	6.1	0.2
	$< \delta >$	(mm/s)	0.24	0.23	0.18	0.18	0.16	0.02
	$< \Delta >$	(mm/s)	–	–	0.58	0.60	0.57	0.02
	$< B_{\mathrm{hf}}^{z} >$	(T)	5.7	6.7	5.1	4.0	–	0.3
^{119}Sn	$< B_{\mathrm{hf}}^{\mathrm{tot}} >$	(T)	5.7	6.7	7.3	7.5	7.7	0.3
	$< \delta >$	(mm/s)	1.78	1.75	1.78	1.80	1.82	0.02
	$< \Delta >$	(mm/s)	–	–	0.82	0.82	0.81	0.05

TABLE II. The average magnetic moments (in μ_B) used in and derived from the present analysis. The σ is the moment of the alloy per magnetic atom. $<\mu_{\mathrm{Fe}}^{\mathrm{tot}}>$ were obtained from the bulk value at $x = 0.000$, and all other moments were derived from the Mössbauer data (detailed description is given in the text). The superscript 'z' denotes longitudinal components (in the direction of domain magnetization σ, or μ_{Fe}^{z}) while 'xy' denotes transverse components and 'tot' is the total moment. The subscript '1' denotes average moment per atom of the first near-neighbour (NN) shell. The transverse components of the average moment on the 1$^{\mathrm{st}}$ NN shell for the non-collinear alloys exhibiting spin-freezing transition (i.e. those with $x = 0.235$ and $x = 0.320$), and of the total average moment of the 1$^{\mathrm{st}}$ NN shell for the complete spin-glass ($x = 0.450$), were also calculated assuming random orientation of transverse components $<\mu_{\mathrm{Fe}}^{\mathrm{xy}}>$ and $<\mu_{\mathrm{Mn}}^{\mathrm{xy}}>$ or total moments $<\mu_{\mathrm{Fe}}^{\mathrm{tot}}>$ and $<\mu_{\mathrm{Mn}}^{\mathrm{tot}}>$ respectively. These values are shown at the bottom of the table. A negative sign means AF alignment with respect to the direction of the corresponding component of the Fe moment.

x	0.000	0.107	0.235	0.320	0.450
σ[a]	2.19 ± 0.01	1.69 ± 0.01	1.07 ± 0.01	0.59 ± 0.01	0.00
$<\mu_{\mathrm{Fe}}^{z}>$	2.19 ± 0.01	2.16 ± 0.01	1.84 ± 0.06	1.47 ± 0.07	–
$<\mu_{\mathrm{Fe}}^{\mathrm{xy}}>$	0.00	0.00	1.04 ± 0.11	1.48 ± 0.06	–
$<\mu_{\mathrm{Fe}}^{\mathrm{tot}}>$	2.19 ± 0.01	2.16 ± 0.01	2.12 ± 0.01	2.09 ± 0.01	2.04 ± 0.01
$<\mu_{\mathrm{Mn}}^{z}>$	–	-3.47 ± 0.50	-3.57 ± 0.35	-3.43 ± 0.25	–
		-2.89 ± 0.10[a]			
$<\mu_{\mathrm{Mn}}^{\mathrm{xy}}>$	–	0.00	-2.39 ± 0.37	-2.25 ± 0.15	–
$<\mu_{\mathrm{Mn}}^{\mathrm{tot}}>$	–	3.47 ± 0.50	4.29 ± 0.57	4.10 ± 0.29	3.28 ± 0.47
		2.89 ± 0.10[a]			
$<\mu_{1}^{z}>$	2.19 ± 0.01	1.56 ± 0.05	0.57 ± 0.07	-0.10 ± 0.07	–
$<\mu_{1}^{\mathrm{xy}}>$	0.00	0.00	0.24 ± 0.02	0.29 ± 0.02	–
$<\mu_{1}^{\mathrm{tot}}>$	2.19 ± 0.01	1.56 ± 0.05	0.62 ± 0.06	0.31 ± 0.03	0.35 ± 0.01
$<\mu_{1random}^{xy}>$	–	–	0.45 ± 0.06	0.52 ± 0.03	–

$<\mu^{tot}_{1random}>$	–	–	–	–	0.80 ± 0.08

[a]Obtained from measurements of bulk magnetization at 5 K extrapolated to zero field.

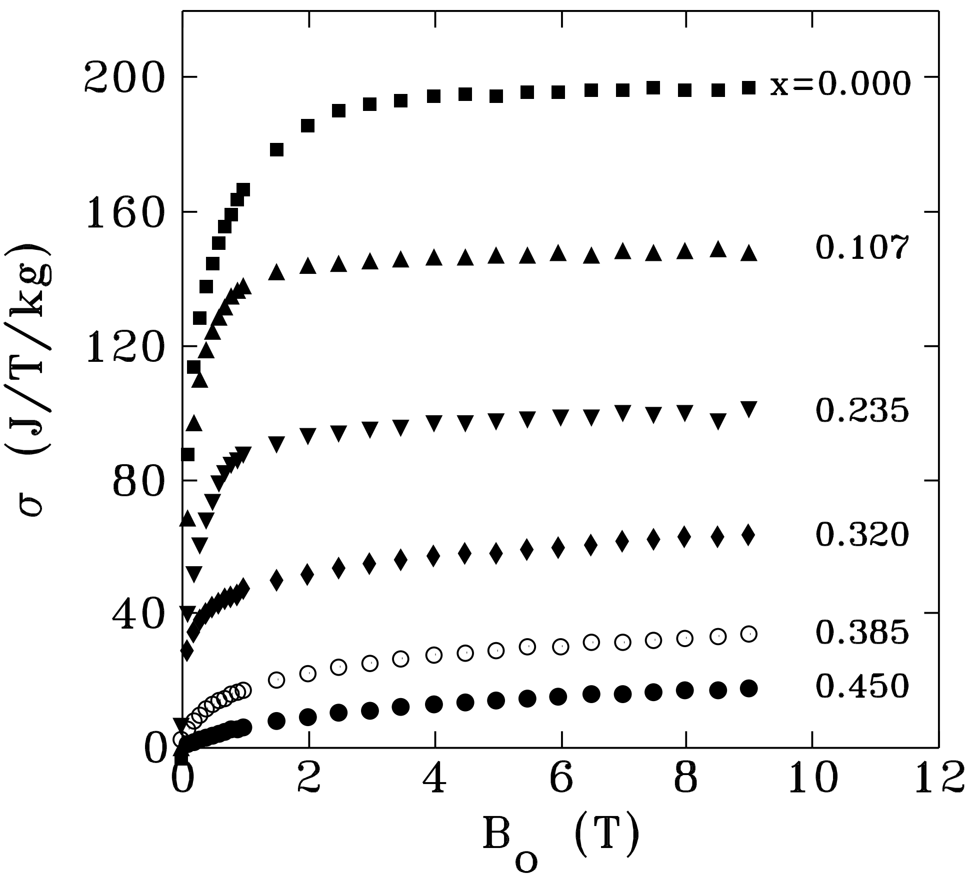

FIG. 1. Magnetization of a$-$($Fe_{1-x}Mn_x$)$_{78}$$Sn_2Si_6B_{14}$ at 5 K as a function of applied magnetic induction.

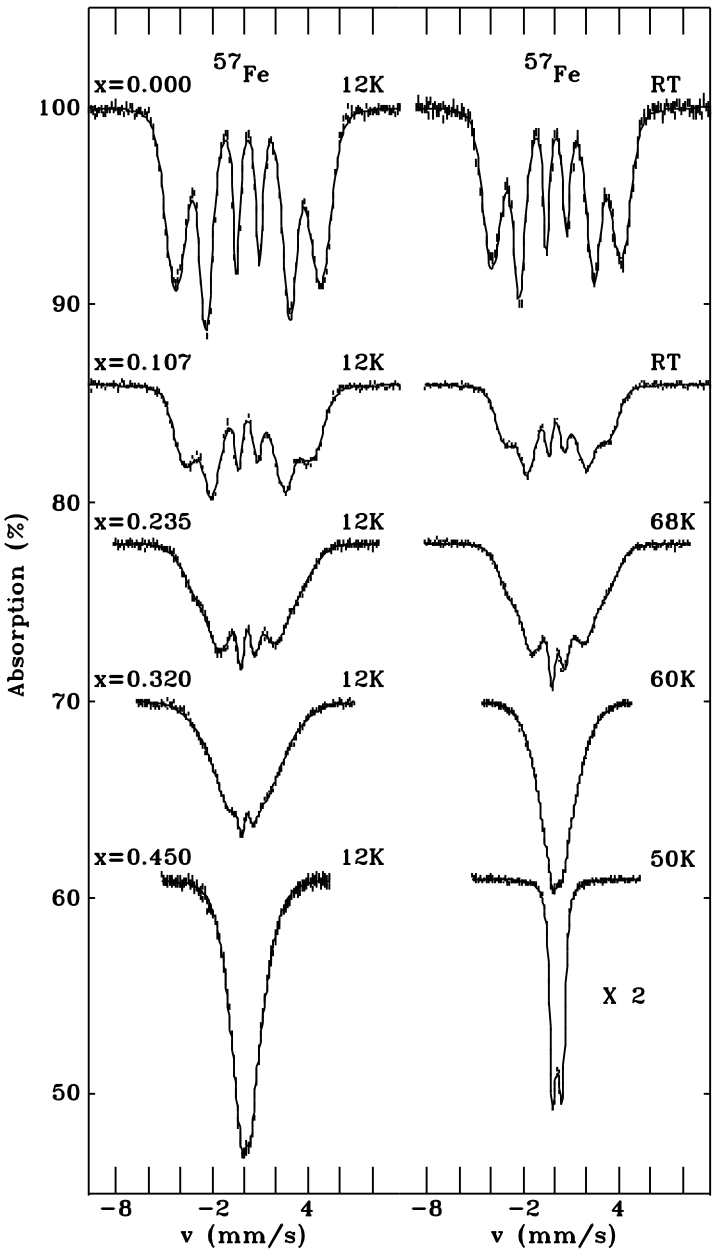

FIG. 2. ^{57}Fe Mössbauer spectra, with fits, of a$-(Fe_{1-x}Mn_x)_{78}Sn_2Si_6B_{14}$ measured at 12 K (left column) and various temperatures (right column) illustrate magnetic state for different compositions: $x = 0.000$, $x = 0.107$ at RT (only a slight reduction of average hyperfine magnetic field), $x = 0.235$, $x = 0.320$ at 68 K and 60 K respectively (just above T_{xy}), $x = 0.450$ at 50 K (complete collapse of magnetic hyperfine splitting above T_c).

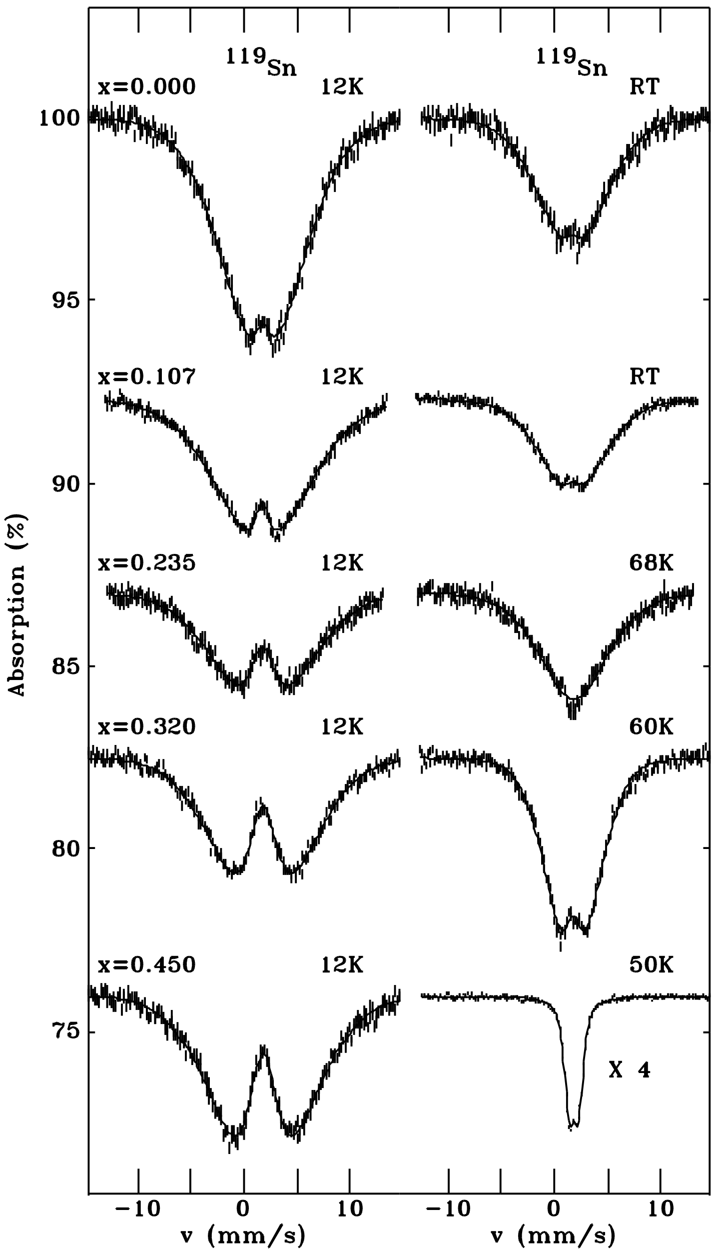

FIG. 3. ^{119}Sn Mössbauer spectra, with fits, of a$-(Fe_{1-x}Mn_x)_{78}Sn_2Si_6B_{14}$ measured at 12 K (left column) and temperatures shown in Fig. 2 (right column) illustrate the transfer of hyperfine fields from magnetic moments of surrounding Fe atoms to the non-magnetic Sn probe.

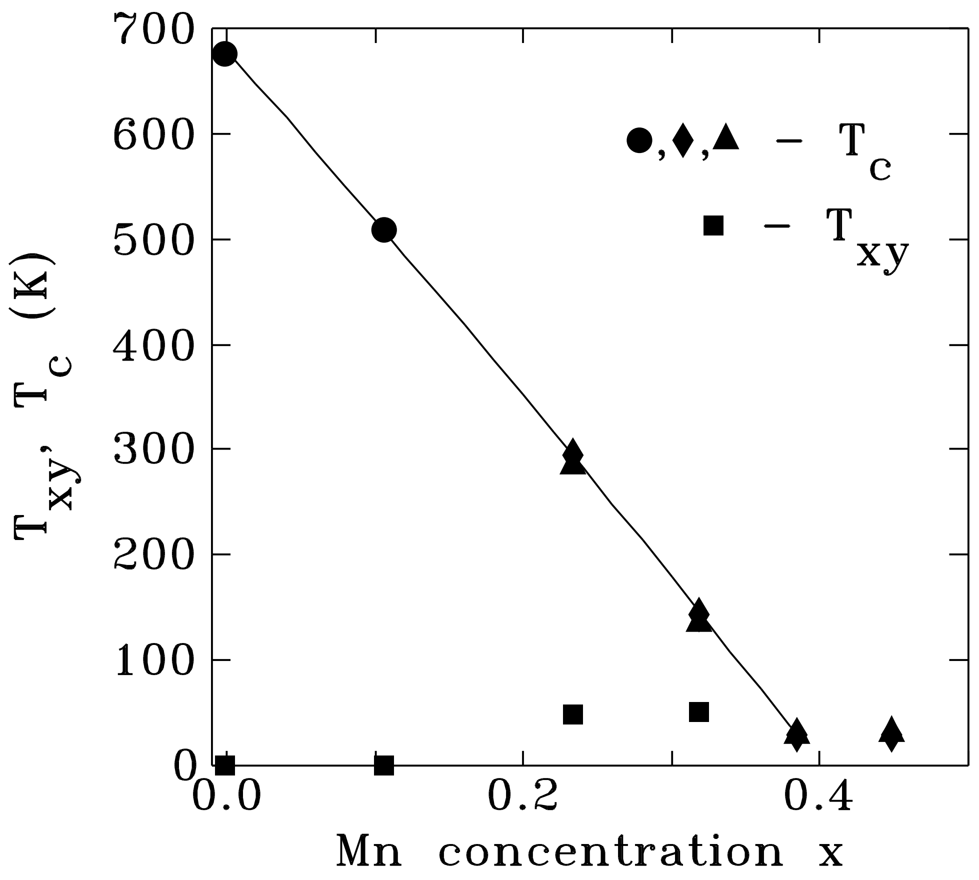

FIG. 4. Magnetic phase diagram for a$-(Fe_{1-x}Mn_x)_{78}Sn_2Si_6B_{14}$ derived from temperature dependences of the average ^{57}Fe hyperfine field (triangles and boxes) and by thermogravimetric analysis (TGA) (circles), and from measurements of bulk magnetization (diamonds).

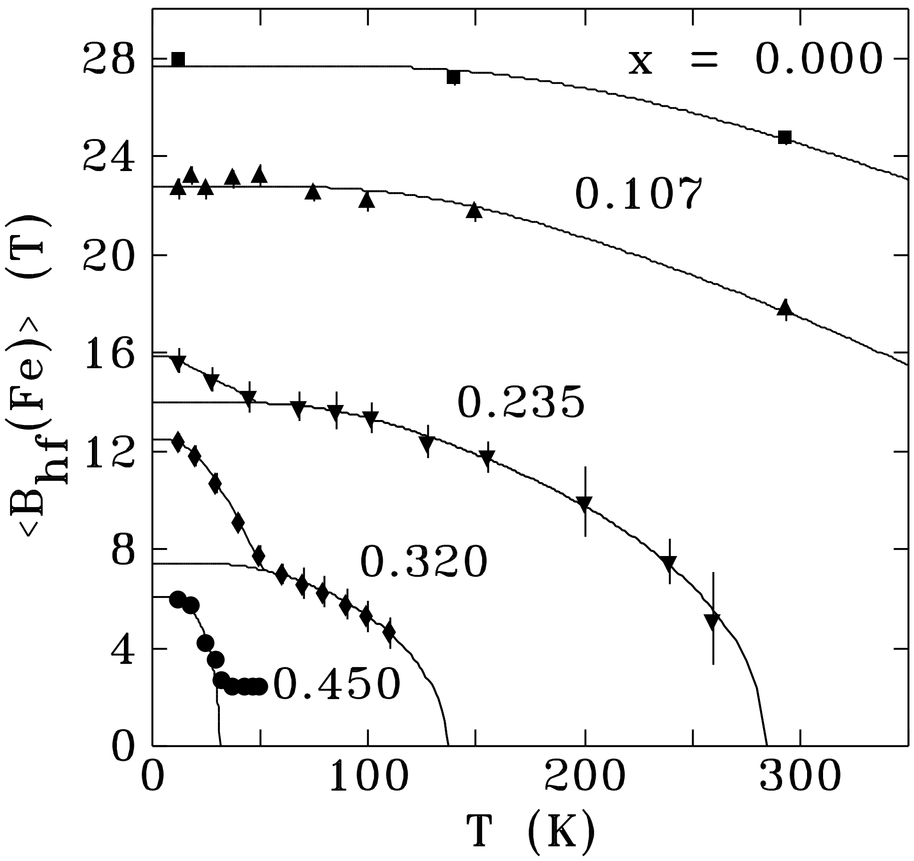

FIG. 5. Average ^{57}Fe hyperfine fields derived from Mössbauer spectra for different compositions of a$-(Fe_{1-x}Mn_x)_{78}Sn_2Si_6B_{14}$. Fits of temperature dependences are also shown. Alloys with $x = 0.000$, $x = 0.107$ and $x = 0.450$ show a smooth temperature dependence which was fitted by a modified Brillouin function, while those with $x = 0.235$ and $x = 0.320$ exhibit a pronounced kink at the transverse spin freezing temperature T_{xy}; fits with a combined modified Brillouin function and linear term are shown below T_{xy} and with a modified Brillouin function only above T_{xy}.

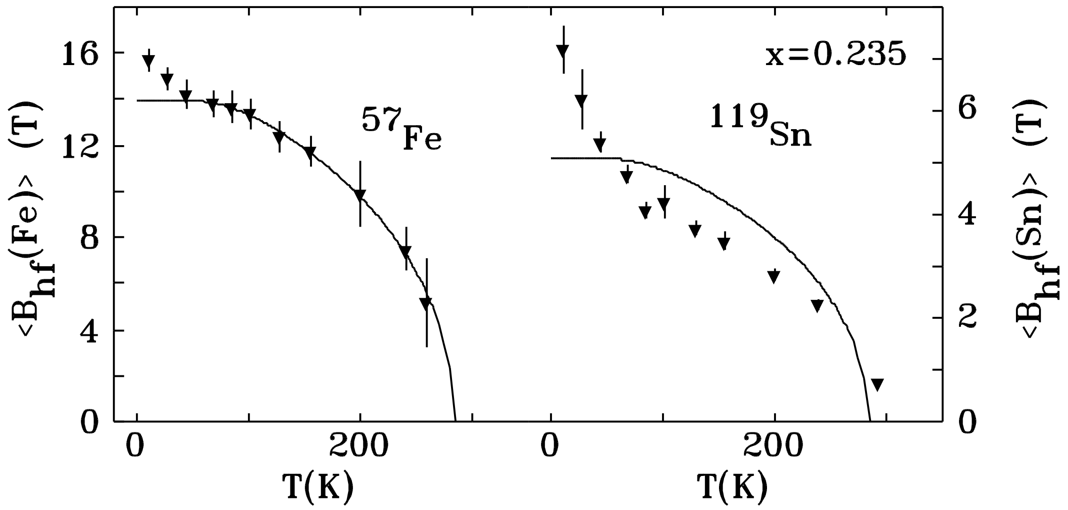

FIG. 6. Comparison of the temperature dependence of the average ^{57}Fe (left) and ^{119}Sn (right) hyperfine fields for a$-(\mathrm{Fe_{1-x}Mn_x})_{78}\mathrm{Sn_2Si_6B_{14}}$ with $x = 0.235$. The fit of the dependence for ^{57}Fe at temperatures above $\mathrm{T_{xy}}$ by a modified Brillouin function is also shown; it is scaled to the $< B^z_{\mathrm{hf}}(Sn) >$ value at T = 0 K on the right. The much steeper decrease in the average ^{119}Sn hyperfine field demonstrates the strong temperature anomaly for ^{119}Sn (see details in the text).

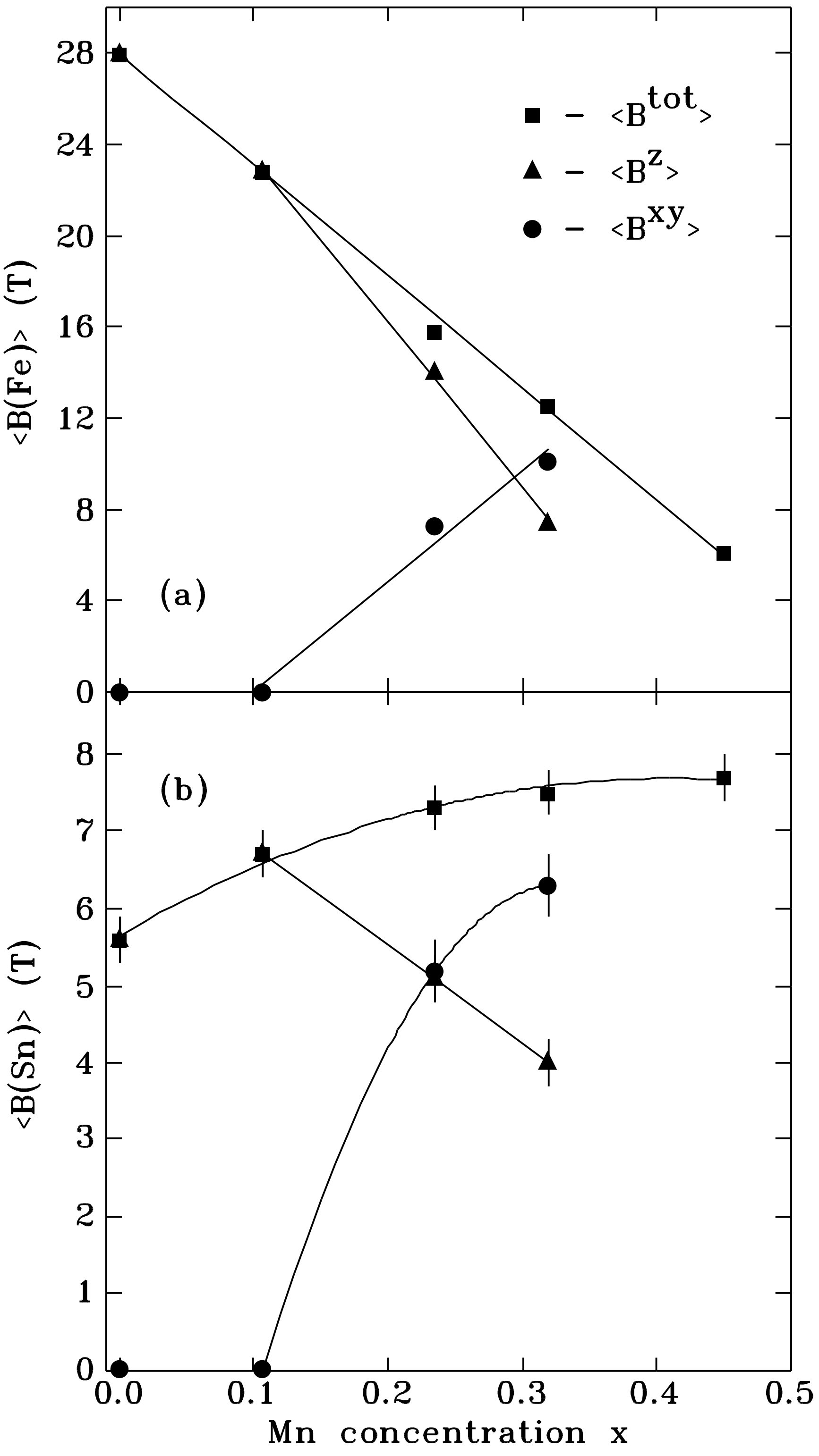

FIG. 7. Concentration dependence of the average $|< B_{\rm hf}^{\rm tot} >|$, $|< B_{\rm hf}^{z} >|$ and $|< B_{\rm hf}^{\rm xy} >|$ extrapolated to zero temperature for ^{57}Fe (a) and ^{119}Sn (b). Solid lines are guides to the eye.

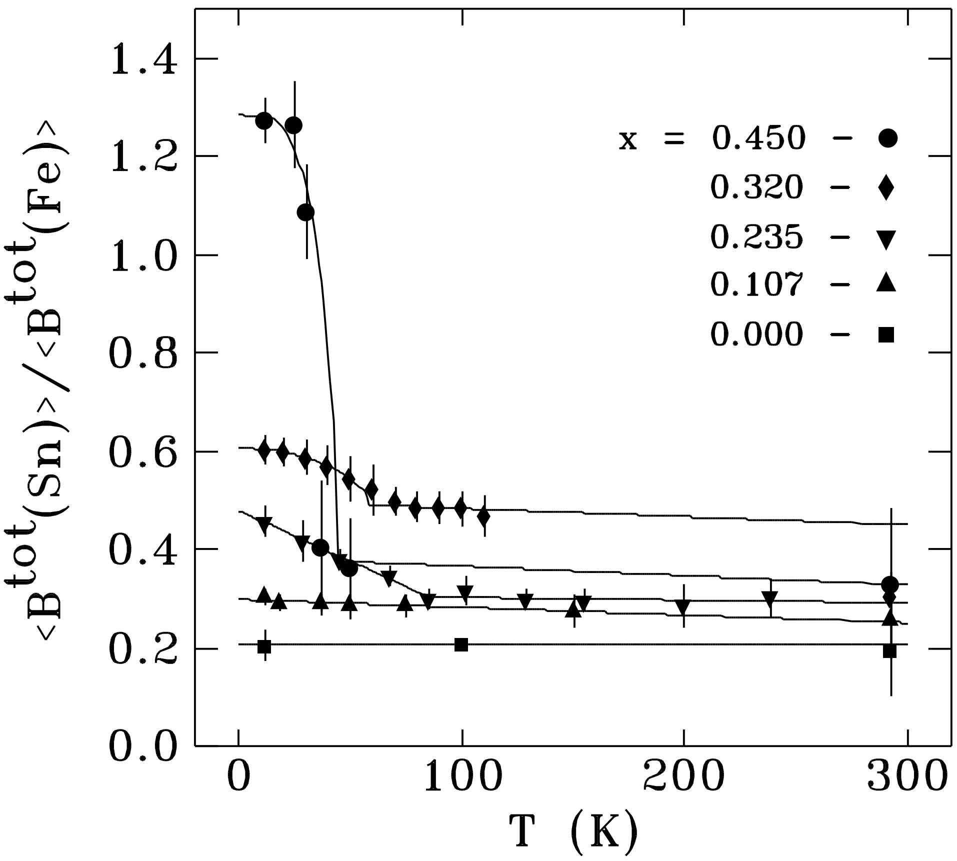

FIG. 8. Ratio of the total average transferred hyperfine field at ^{119}Sn sites to that at the ^{57}Fe sites as a function of temperature for different compositions of a$-(Fe_{1-x}Mn_x)_{78}Sn_2Si_6B_{14}$. Solid lines are guides to the eye.

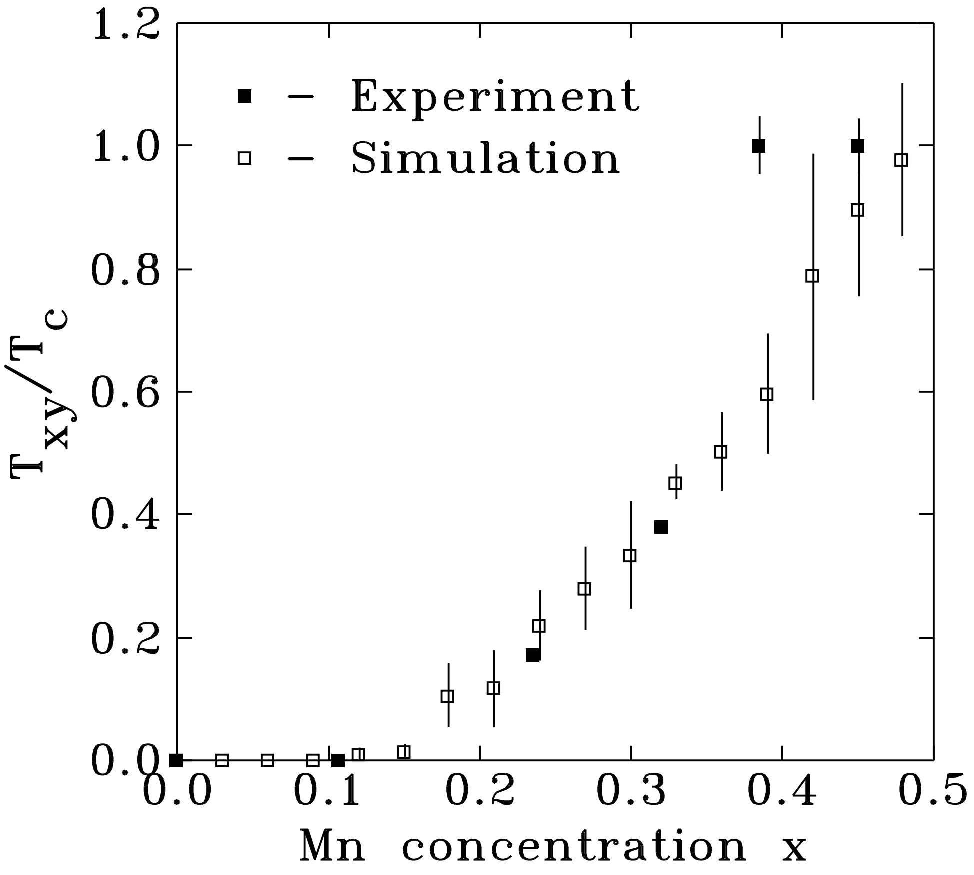

FIG. 9. Normalized Comparison of magnetic phase diagram for a$-(Fe_{1-x}Mn_x)_{78}Sn_2Si_6B_{14}$ (solid symbols) with that derived from Monte Carlo simulations on a simple cubic site disordered Heisenberg model with nearest-neighbor interactions (open symbols) [5]. Note excellent agreement with the main predictions of the simulations. Note also that at $x = 0.385$ a$-(Fe_{1-x}Mn_x)_{78}Sn_2Si_6B_{14}$ has already reached spin-glass state. This discrepancy is probably caused by inequality of absolute values of coupling constants $J_{\rm FeFe}$, $J_{\rm MnMn}$, and $J_{\rm FeMn}$, which were assumed to be $+1$, -1 and -1 respectively in the numerical work.